

RESEARCH PAPER

Assessment of pulmonary mucociliary transport using magnetic nanoparticles: influence of their surface potential

Kohei Nishimoto¹, Satoshi Nagano², Kenya Murase^{1,2*}

¹Department of Medical Physics and Engineering, Division of Medical Technology and Science, Faculty of Health Science, Graduate School of Medicine, Osaka University, Suita, Osaka, Japan

²Global Center for Medical Engineering and Informatics, Osaka University, Suita, Osaka, Japan

ABSTRACT

Objective(s): Inhaled aerocontaminants are removed from the lungs by pulmonary mucociliary transport (MCT) as an important defense mechanism. This study was undertaken to investigate the influence of the surface potential of magnetic nanoparticles (MNPs) on the MCT in murine lungs by use of magnetic particle imaging (MPI).

Materials and Methods: Three kinds of MNPs (carboxymethyl dextran magnetite (CM), alkali-treated dextran magnetite (AM), and trimethylammonium dextran magnetite (TM)) with almost the same hydrodynamic diameters (50-55 nm) but different surface (zeta) potentials (-24 mV for CM, -15 mV for AM, and +2 mV for TM) were intratracheally injected to anesthetized ICR male mice at 10 weeks old using a nebulizing microsyringe containing 50 μ L of MNPs. MPI images were acquired at 0.5, 6, 24, 72, and 168 hours after the injection of agents for each mouse. The retention value of the MNPs in the lungs was quantified from the average pixel value of the lungs in the MPI image.

Results: The retention value of TM in the lungs was significantly greater than that of AM at 6 and 168 hours after the injection of agents, and was significantly greater than that of CM at 72 and 168 hours after injection. The retention value of AM was significantly greater than that of CM at 168 hours after injection.

Conclusion: The surface potential of MNPs affects the clearance of MNPs from the lungs due to MCT, suggesting that the retention of MNPs in the lungs can be controlled by manipulating the surface potential of MNPs. MPI will be useful for the visual and quantitative assessment of MCT, because MPI allows for repeated and long-term studies with a single injection of MNPs and with no radiation exposure.

Keywords: Magnetic nanoparticles, Magnetic particle imaging, Pulmonary mucociliary transport, Surface potential

How to cite this article

Nishimoto K, Nagano S, Murase K. Assessment of pulmonary mucociliary transport using magnetic nanoparticles: influence of their surface potential. *Nanomed J.* 2019; 6(3):161-166. DOI: 10.22038/nmj.2019.06.00002

INTRODUCTION

Inhaled aerocontaminants are removed from the lungs by pulmonary mucociliary transport (MCT) as an important and non-specific defense mechanism. Mucus secreted from airway goblet cells and gland cells traps the inhaled particles, and the trapped particles are transported from the peripheral lungs through the airways and larynx into the gastrointestinal tract by the coordinated motion of cilia beating [1, 2].

Magnetic-controlled drug delivery is one of the most promising therapeutic approaches for cancer and/or severe diseases, because this approach

can increase the efficacy of drugs and decrease their adverse effects [3]. As drugs can be directly delivered to the lungs via the trachea, delivery to the respiratory organs has also attracted great interest [4, 5]. Although the application of nanoparticles has attracted a great deal of attention, some reports have expressed concern about the influence of the inhaled nanoparticles on the lungs [6, 7]. Thus, when considering magnetic-controlled drug delivery to the lungs using magnetic nanoparticles (MNPs), it is important to evaluate the retention and clearance of MNPs in the lungs. Nanometer-sized particles can reach the lung periphery more easily than micrometer-sized particles, because there are few effects of inertial impaction and sedimentation on the nanometer-

* Corresponding Author Email: murase@sahs.med.osaka-u.ac.jp
Note. This manuscript was submitted on February 3, 2019; approved on May 15, 2019

sized particles [8]. Although the dependence of pulmonary clearance on the diameter of inhaled particles is well known [8], its dependence on other factors has not been fully clarified yet. Further investigations on the distribution and clearance of MNPs in the lungs are needed.

Methods using radionuclides such as technetium-99m have been commonly utilized in the clinical setting to measure MCT [9, 10]. The use of these methods, however, is limited by several factors. In examinations using radionuclides, radiation exposure to patients and medical staff is unavoidable. The short half-lives of radionuclides also make long-term observation difficult, because their radioactivities attenuate with time. In addition, the use of radionuclides is strictly regulated and is limited to radiation-control areas.

The magnetic particle imaging (MPI) method was firstly launched in 2005 [11]. In MPI, the nonlinear response of MNPs to an external magnetic field is used for image formation, and the spatial distribution of MNPs can be visualized with high sensitivity and spatial resolution and in positive contrast, unlike magnetic resonance imaging (MRI). MPI can also quantify the content of MNPs because the concentration of MNPs linearly correlates with the pixel value of the corresponding MPI image [12]. Moreover, long-term *in vivo* monitoring of MNPs can be realized using MPI, because non-attenuating and radiation-free MNPs are used as a signal source in MPI. We previously attempted to image the lungs using MPI and nebulized MNPs, and succeeded in visualizing the spatial distribution of MNPs in the murine lungs using MPI [13].

This study was undertaken to investigate the influence of the surface potential of MNPs on the pulmonary MCT in mice using MPI.

MATERIALS AND METHODS

Magnetic nanoparticles (MNPs)

Three kinds of MNPs with different surface (zeta) potentials (carboxymethyl dextran magnetite (CM), alkali-treated dextran magnetite (AM), and trimethylammonium dextran magnetite (TM)) were purchased from Meito Sangyo Co., Ltd. (Aichi, Japan). CM is a magnetite (Fe_3O_4) which has carboxylic groups in the repetitive units [14]. AM is a magnetite having a carboxylic group at its reduction end and is synthesized by heat treatment of dextran in a sodium hydroxide solution [14]. TM is a magnetite whose surface

is positively charged by coating it with tertiary amine [15]. The mean hydrodynamic diameters and surface (zeta) potentials of these MNPs are summarized in Table 1 [15].

Table 1. Mean hydrodynamic diameters and surface (zeta) potentials of three kinds of magnetic nanoparticles [15]. CM: carboxymethyl dextran magnetite, AM: alkali-treated dextran magnetite, and TM: trimethylammonium dextran magnetite

	CM	AM	TM
Mean hydrodynamic diameter [nm]	50	55	54
Zeta potential [mV]	-24	-15	+2

Magnetic particle imaging (MPI) system

Fig 1 shows a photograph of our MPI scanner. Our MPI system is described in details in our previous papers [16-18]. Briefly, a field-free line (FFL) was formed at the center of the selection magnetic field, which was generated by two neodymium magnets placed opposite each other (Fig 1). The spatial encoding was performed using the FFL. The strengths of the selection magnetic field gradient perpendicular and parallel to the FFL were 3.9 T/m and 0.1 T/m, respectively. The drive magnetic field was generated by an excitation (solenoid) coil, which was placed between the two neodymium magnets (Fig 1). The length, inner diameter, and outer diameter of the excitation coil were 100 mm, 80 mm, and 110 mm, respectively. The frequency and peak-to-peak strength of the drive magnetic field were taken as 400 Hz and 20 mT, respectively [16]. The signals from the MNPs were received by a gradiometer-type receiving coil. The length, inner diameter, and outer diameter of the receiving coil were 50 mm, 35 mm, and 40 mm, respectively. The receiving coil was placed inside the excitation coil (Fig 1), from which the third-harmonic signals were extracted using a lock-in amplifier (LI5640, NF Co., Kanagawa, Japan) and transformed to digital data by a personal computer connected to a multifunction data acquisition device (USB-6212, National Instruments Co., Ltd., TX, USA).

Projection data for image formation were acquired by automatically rotating both a mouse and the receiving coil around the receiving coil axis through 180° in steps of 5° and translating them in the direction perpendicular to the receiving coil axis from -16 mm to $+16$ mm in steps of 1 mm, using an XYZ-axes rotary stage (HPS80-50X-M5, Sigma Koki Co., Tokyo, Japan) (Fig 1). The rotation and translation of the XYZ-axes rotary stage (Fig

1) were controlled using LabVIEW (National Instruments Co., Ltd., TX, USA) [17].

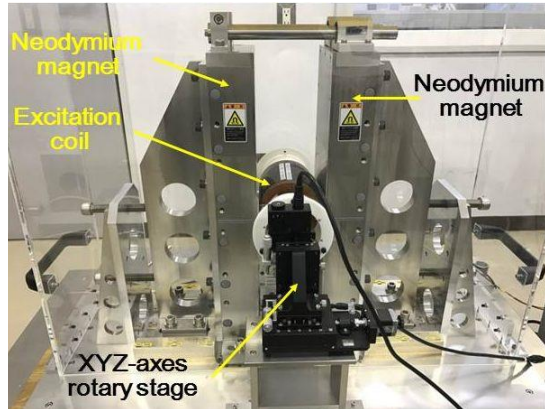


Fig 1. Photograph of our scanner for magnetic particle imaging (MPI). A field-free line is formed at the center of two neodymium magnets placed opposite each other. A drive magnetic field for inducing MPI signals is generated by an excitation coil and the MPI signals are received by a gradiometer-type receiving coil placed inside the excitation coil. Projection data for image formation are acquired by automatically rotating both a mouse and the receiving coil and translating them using an XYZ-axis rotary stage

After each projection data set was converted into 64 bins by linear interpolation, and both the feedthrough interference and inhomogeneous sensitivity of the receiving coil were corrected [17], MPI images (transverse images) were obtained from the projection data. For image reconstruction, the maximum likelihood-expectation maximization (ML-EM) algorithm was used, in which the number of iterations was taken as 15 [16-18].

Animal experiments

All animal experiments were carried out after their procedures were approved by the animal ethics review committee at Osaka University School of Medicine. ICR (Institute of Cancer Research) male mice at 9 weeks old were purchased from Japan SLC, Inc. (Shizuoka, Japan). Before starting the experiment, the mice were habituated to the rearing environment for one week. The mice were allowed free access to water and food for 24 hours, and were kept under standard laboratory conditions (room temperature at 22-23 °C, around 50% humidity, and a 12:12-hour light-dark cycle).

After habituation for one week, the mice were randomly divided into three groups: CM group (n = 7), AM group (n = 6), and TM group (n = 7).

The mice in the CM, AM, and TM groups were intratracheally injected with CM, AM, and TM, respectively. The injected volume was fixed at 50 μ L in all cases.

The intratracheal injection of the above agents was conducted using a nebulizing microsyringe (Penn-Century Inc., PA, USA) connected to a high-pressure syringe under anesthesia using pentobarbital sodium (Somnopentyl, Kyoritsu Seiyaku Co., Tokyo, Japan) (0.012 mL/g body weight). To properly administer the above agents into the trachea, the tip of the microsyringe was introduced into the trachea of a mouse using a dedicated laryngoscope [13].

To follow up the subsequent change in the distribution of MNPs in the lungs, MPI studies were carried out at 0.5, 6, 24, 72, and 168 hours after the injection of agents for each mouse. After the MPI studies, X-ray CT images were also acquired using a 4-row multi-slice CT scanner (Asteion, Toshiba Medical Systems Co., Tochigi, Japan). The tube voltage, tube current, and slice thickness in the X-ray CT studies were taken as 120 kV, 210 mA, and 0.5 mm, respectively. For anatomical identification, the MPI images were co-registered to the corresponding X-ray CT images using the rotation and translation parameters previously obtained by a three-line phantom [12, 13].

data and statistical analyses

In the present study, the pixel value of the MPI image was referred to as the MPI value. To calculate the average MPI value, a region of interest (ROI) was drawn on the lungs in each MPI image. When extracting the contour of the lungs in the MPI image, the threshold value was taken as 30% of the maximum MPI value within the ROI.

The retention value of the MNPs in the lungs was quantified by dividing the average MPI value obtained from each MPI study by that obtained from the initial MPI study at 0.5 hours after the injection of agents.

One-way analysis of variance (ANOVA) was conducted to compare the retention values among groups and significance was examined by Tukey's multiple comparison tests. If a *p* value was less than 0.05, it was considered significant.

RESULTS

Fig 2 shows typical fused images between the MPI and X-ray CT images in the CM group (upper row), the AM group (middle row), and the TM

group (lower row) at 0.5, 6, 24, 72, and 168 hours after the injection of agents.

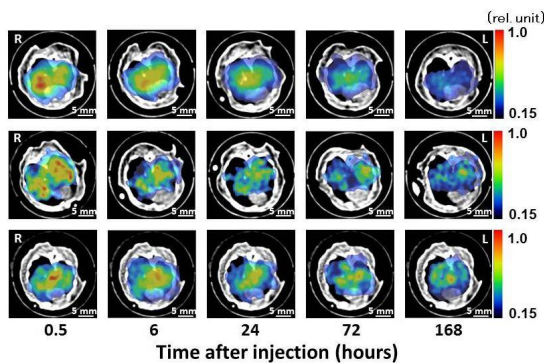


Fig 2. Typical fused images between the MPI and X-ray CT images in the CM (upper row), AM (middle row), and TM groups (lower row) at 0.5, 6, 24, 72, and 168 hours after the injection of agents. The mice in the CM, AM, and TM groups were intratracheally injected with carboxymethyl dextran magnetite, alkali-treated dextran magnetite, and trimethylammonium dextran magnetite, respectively. The lowest and highest intensity levels for displaying MPI images were set to be the same. Scale bar = 5 mm

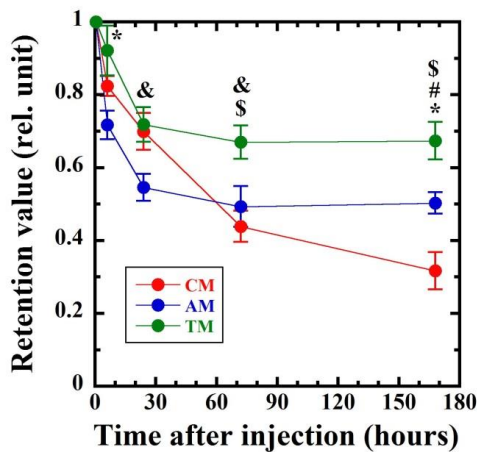


Fig 3. Time courses of the retention values of magnetic nanoparticles in the lungs in the CM (red circles, $n = 7$), AM (blue circles, $n = 6$), and TM groups (green circles, $n = 7$). Each retention value was quantified by dividing the average MPI value obtained from each MPI study by that obtained from the initial MPI study at 0.5 hours after the injection of agents. Data are represented by the mean \pm standard error. #: $p < 0.05$ between the AM and CM groups. *: $p < 0.05$ between the AM and TM groups. \$: $p < 0.05$ between the TM and CM groups. &: $0.05 < p < 0.1$ between the AM and TM groups

As shown in Fig 2, the temporal changes of the MPI images differed depending on the MNPs administered to the lungs.

The MPI images in the CM group (upper row) did not show rapid decreases in MPI values for the first 6 hours, but decreased slowly with time thereafter. In contrast, the MPI images in the TM group (lower row) showed MPI values to decrease slightly for the first 6 hours and then remain almost constant up to 168 hours.

Fig 3 shows the time courses of the retention values of the MNPs in the lungs in the CM group (red circles, $n = 7$), the AM group (blue circles, $n = 6$), and the TM group (green circles, $n = 7$). The retention value in the TM group was significantly greater ($p < 0.05$) than that in the AM group at 6 and 168 hours after the injection of agents. Although there was a tendency for the retention value in the TM group to be greater than that in the AM group at 24 hours ($0.05 < p < 0.1$) and 72 hours ($0.05 < p < 0.1$) after injection, the differences were not significant.

The retention value in the TM group was also significantly greater ($p < 0.05$) than that in the CM group at 72 and 168 hours after injection. The retention value in the AM group was significantly greater ($p < 0.05$) than that in the CM group at 168 hours after injection.

DISCUSSION

The present study investigated the time-dependent changes of MNPs administered intratracheally to the murine lungs using MPI, and evaluated the influence of the surface potential of MNPs on the pulmonary MCT. We previously reported that the average MPI value linearly correlated with the iron concentration of MNPs in phantom studies [12]. From these results, the change of the MPI value is considered to reflect that in the content of MNPs. Therefore, it appears to be possible to quantitatively evaluate the temporal change of MNPs in the lungs using the MPI value. Our results (Figs 2 and 3) demonstrated that MPI is of use for visualizing the distribution of MNPs in the lungs and is applicable to quantitative assessment of the function of MCT.

In this study, we investigated the influence of the surface potential of MNPs on pulmonary MCT by using three kinds of MNPs with different surface (zeta) potentials (-24 , -15 , and $+2$ mV), while adjusting their mean hydrodynamic diameters to be almost the same (50-55 nm) to minimize the size effect of MNPs (Table 1). As shown in Fig 2, the MPI value tended to decrease with time in all groups, although the time course of decrease

differed among the MNP types. In the CM group, the MPI value did not show rapid clearance for the first 6 hours, but decreased slowly with time thereafter. In contrast, the MPI value in the TM group decreased slightly for the first 6 hours and then remained almost constant up to 168 hours. When the retention value of the MNPs in the lungs was quantified from the average MPI values (Fig 3), the retention value of positively-charged MNPs was greater than that of negatively-charged MNPs, because the retention value in the TM group was significantly greater than those in the AM group at 6 and 168 hours and in the CM group at 72 and 168 hours after the injection of agents. These results suggest that the difference in the retention of MNPs observed in this study was mainly due to the differences in surface potential of MNPs, and that the retention of MNPs can be controlled by changing the surface potential of MNPs.

Chen *et al.* reported that positively-charged nanoparticles promoted the aggregation of mucin, thereby reducing its hydration and diffusivity [19]. As described above, the retention value of the positively-charged MNPs (TM) was greater than those of other MNPs (Fig 3). Thus, it appears that the greater retention of TM was mainly due to the reduction in hydration and diffusivity of mucin and consequent formation of MNPs-mucin gel complexes. In addition, Chen *et al.* reported that negatively-charged (carboxyl- functionalized) nanoparticles may promote the dispersion of mucin gels by enhancing the network hydration [20]. From the consistency between the results obtained in this study (Figs 2 and 3) and those reported by Chen *et al.* [19, 20], the observed differences in the retention among the MNPs with different surface potentials may be due to the fact that the surface potential of MNPs affects the aggregation, hydration, and dispersion of mucin.

It is known that besides MCT, alveolar macrophages are also involved in the clearance mechanism of the lungs. The alveolar macrophages (also known as dust cells) are a type of macrophages (phagocytic cells derived from monocytes) found in the pulmonary alveoli near the pneumocytes and are responsible for removing inhaled particles such as dust or microorganisms from the respiratory surfaces [21]. The alveolar macrophages, however, have a size-discriminating property such that the size of particles they engulf is relatively large, ranging from approximately 1.5 μm to 3 μm [21]. Thus, it appears that the

nanometer-sized particles used in this study (Table 1) are not efficiently phagocytosed by alveolar macrophages, and that the temporal changes of MNPs observed in this study (Figs 2 and 3) were mainly due to MCT; the contribution of alveolar macrophages was small.

The greater retention associated with the positive surface potential of MNPs (Figs 2 and 3) may be useful for lung cancer therapy using inhaled drugs, which would be of benefit to patients by sustaining high drug concentration in the lung tissue and lowering systemic drug exposure [22]. To reduce side effects, however, it would not be desirable for the inhaled drugs to remain in the lungs for a long time [23]. The present results suggest that the retention of MNPs in the lungs can be controlled according to the purpose by manipulating the surface potential of MNPs. When considering the control of retention of MNPs in the lungs, MPI will be useful for monitoring the effect of the control and feeding-back the result to the control, because MPI can be carried out in a repetitive manner with a single administration of MNPs and with no radiation exposure.

CONCLUSION

The present results demonstrated that the surface potential of MNPs affects the clearance of MNPs from the lungs due to MCT; making the surface potential more positive reduces the clearance of MNPs from the lungs, suggesting that the retention of MNPs in the lungs can be controlled by manipulating the surface potential of MNPs. Because MPI allows for repeated and long-term studies with a single administration of MNPs and without radiation exposure, it will be useful for the visual and quantitative assessment of MCT.

ACKNOWLEDGEMENTS

This study was supported by JSPS (the Japan Society for the Promotion of Science) KAKENHI Grant Numbers 25282131 and 15K12508. This study was also supported by the Japan Science and Technology Agency (JST).

DECLARATION OF INTEREST

The authors declare no conflicts of interest associated with this manuscript.

REFERENCES

1. Clarke SW, Pavia D. Lung mucus production and mucociliary

- clearance: methods of assessment. *Br J Clin Pharmacol.* 1980; 9: 537-546.
- Antunesa MB, Cohen NA. Mucociliary clearance - a critical upper airway host defense mechanism and methods of assessment. *Curr Opin Allergy Clin Immunol.* 2007; 7: 5-10.
 - Mikhaylov G, Mikac U, Magaeva AA, Itin VI, Naiden EP, Psakhye I, Babes L, Reinheckel T, Peters C, Zeiser R, Bogyo M, Turk V, Psakhye SG, Turk B, Vasiljeva O. Ferriliposomes as an MRI-visible drug-delivery system for targeting tumours and their microenvironment. *Nature Nanotechnol.* 2011; 6: 594-602.
 - Kuzmov A, Minko T. Nanotechnology approaches for inhalation treatment of lung diseases. *J Control Release.* 2015; 219: 500-518.
 - Banura N, Murase K. Magnetic particle imaging for aerosol-based magnetic targeting. *Jpn J Appl Phys.* 2017; 56.
 - Srinivas A, Rao PJ, Selvam G, Goparaju A, Murthy PB, Reddy PN. Oxidative stress and inflammatory responses of rat following acute inhalation exposure to iron oxide nanoparticles. *Hum Exp Toxicol.* 2012; 31: 1113-1131.
 - Sadeghi L, Yousefi BV, Espanani HR. Toxic effects of the Fe₂O₃ nanoparticles on the liver and lung tissue. *Bratisl Lek Listy.* 2015; 116: 373-378.
 - Lippmann M, Yeates DB, Albert RE. Deposition, retention, and clearance of inhaled particles. *Br J Ind Med.* 1980; 37: 337-362.
 - Karacavus S, Intepe YS. The role of Tc-99m DTPA aerosol scintigraphy in the differential diagnosis of COPD and asthma. *Clin Respir J.* 2015; 9: 189-195.
 - Fleming J, Conway J, Majoral C, Tossici-Bolt L, Katz I, Caillibotte G, Perchet D, Pichelin M, Muellinger B, Martonen T, Kroneberg P, Apiou-Sbirlea G. The use of combined single photon emission computed tomography and x-ray computed tomography to assess the fate of inhaled aerosol. *J Aerosol Med Pulm Drug Deliv.* 2011; 24: 49-60.
 - Gleich B, Weizenecker J. Tomographic imaging using the nonlinear response of magnetic particles. *Nature.* 2005; 435: 1214-1217.
 - Murase K, Aoki M, Banura N, Nishimoto K, Mimura A, Kuboyabu T, Yabata I. Usefulness of magnetic Particle Imaging for Predicting the Therapeutic Effect of Magnetic Hyperthermia. *Open J Med Imaging.* 2015; 5: 85-99.
 - Nishimoto K, Mimura A, Aoki M, Banura N, Murase K. Application of magnetic particle imaging to pulmonary imaging using nebulized magnetic nanoparticles. *Open J Med Imaging.* 2015; 5: 49-55.
 - Herrera AP, Barrera C, Rinaldi C. Synthesis and functionalization of magnetite nanoparticles with aminopropylsilane and carboxymethyl dextran. *J Mater Chem.* 2008; 18: 3650-3654.
 - Oishi K, Miyamoto Y, Saito H, Murase K, Ono K, Sawada M, Watanabe M, Noguchi Y, Fujiwara T, Hayashi S, Noguchi H. In vivo imaging of transplanted islets labeled with a novel cationic nanoparticle. *PLoS ONE.* 2013; 8(2): e57046.
 - Murase K, Hiratsuka S, Song R, Takeuchi Y. Development of a system for magnetic particle imaging using neodymium magnets and gradiometer. *Jpn J Appl Phys.* 2014; 53: 067001.
 - Murase K, Banura N, Mimura A, Nishimoto K. Simple and practical method for correcting the inhomogeneous sensitivity of a receiving coil in magnetic particle imaging. *Jpn J Appl Phys.* 2015; 54: 038001.
 - Murase K, Song R, Hiratsuka K. Magnetic particle imaging of blood coagulation. *Appl Phys Lett.* 2014; 104: 2524409.
 - Chen EYT, Wang YC, Chen CS, Chin WC. Functionalized positive nanoparticles reduce mucin swelling and dispersion. *PLoS ONE.* 2010; 5: e15434.
 - Chen EY, Daley D, Wang YC, Garnica M, Chen CS, Chin WC. Functionalized carboxyl nanoparticles enhance mucus dispersion and hydration. *Sci Rep.* 2012; 2: 211.
 - El-Sherbiny IM, El-Baz NM, Yacoub MH. Inhaled nano- and microparticles for drug delivery. *Glob Caridol Sci Pract.* 2015; 2: 1-14.
 - Roa WH, Azarmi S, Al-Hallak MHDK, Finlay WH, Magliocco AM, Löbenberg R. Inhalable nanoparticles, a non-invasive approach to treat lung cancer in a mouse model. *J Control Release.* 2011, 150: 49-55.
 - Woods A, Ptel A, Spina D, Riffo-Vasquez Y, Babin-Morgan A, de Rosales RTM, Sunassee K, Clark S, Cllins H, Bruce K, Dailey LA, Forbes B. In vivo biocompatibility, clearance, and biodistribution of albumin vehicles for pulmonary drug delivery. *J Control Release.* 2015; 210: 1-9.